PAPER

Check for updates

Nonlinear optical properties of porphyrin-based covalent organic frameworks determined by steric-orientation of conjugation†

Bin Liang,[ac] Jie Zhao,[c] Jingjing Wang,[c] Yunfei Li, [ID][c] Bin Han,[b] Jie Li, [ID] *[a] Xu Ding,*[b] Zheng Xie, [ID] *[c] Hailong Wang [ID][b] and Shuyun Zhou[c]

The influences of conjugation on the third-order nonlinear optical (NLO) properties of covalent organic frameworks (COFs) provide guidelines to design the structures for desired applications. In this work, two two-dimensional (2D) porphyrin-based COFs and corresponding topological polymerized three-dimensional (3D) materials have been prepared. Theoretical calculations and experimental results revealed that the linkages between the porphyrins played critical roles in the degree and orientation of conjugation. The topological polymerization of diacetylenyl groups led to increased conjugation of the structures but disturbed the delocalization of the 2D π-conjugation planes. As a result, the 2D COFs with well extended π-conjugated planes exhibited more excellent third-order nonlinear optical properties and stronger excited-state absorption. This work would provide valuable inspiration for the subsequent investigation on the structure–activity relationships by adjusting the conjugation orientation of COFs.

Introduction

Nonlinear optical (NLO) materials are essential in the fields of laser modulation and protection,[1–4] biomedical sciences,[5,6] optical communications,[7–9] and sensors.[10–12] In particular, materials with optical limiting (OL) properties can absorb large amounts of high-energy lasers to reduce output energy, which shows critical application in protecting human eyes and optical devices from laser damage.[13–17] Since covalent organic frameworks (COFs) were first synthesized in 2005,[18] they have been extensively studied in the fields of catalysis,[19,20] adsorption,[21,22] gas separation[23,24] and photovoltaics.[25,26] COFs are those reticular two- and three-dimensional (2D and 3D) organic polymers with long-range well-defined structures and rich porosity,[27,28]

and diverse functionalities can be accessed by predesigning and post-modifying the covalent-linked frameworks.[29–31] Due to the highly delocalized π-conjugated planes, COFs based on porphyrins exhibit large and fast NLO response, and have been widely involved in the NLO field together the large conjugated building covalently bonded together. In 2019, Feng *et al.* first reported bismetalloporphyrin-based two-dimensional (2D) COFs.[32] They achieved a high nonlinear absorption coefficient (β = 4470 cm GW^{-1}) and intensity-dependent NLO switching behavior due to the effective π-conjugated structures and charge transport abilities. Biswal *et al.* reported another kind of porphyrin-based 2D COFs with equally excellent NLO properties by replacing the connecting unit with a thiazolo[5,4-d]thiazole unit.[33] Chen *et al.* first synthesized an ether-linked porphyrin-based 2D COF which realized the switch of the NLO response in a broad range from visible light to the near infrared region.[34]

The effect of conjugation of small organic molecules on their nonlinear absorption has been studied extensively.[35–37] (1) By extending the π-conjugated length, the molecules would have high transition dipole moments and narrow linewidth, which endow them with stronger nonlinear absorption.[38,39] (2) The conjugation of molecules was also affected by their planar conformation. When planar rigidity of the molecule was stronger, the electronic coupling would be optimized and the overlap of π-orbitals was inseparable.[40,41] (3) When the central connecting bridges were converted into more conjugate ethylene

[a] *Key Laboratory of Interface Science and Engineering in Advanced Materials, Ministry of Education, Taiyuan University of Technology, Taiyuan, 030024, China. E-mail: lijie01@tyut.edu.cn*

[b] *Beijing Advanced Innovation Center for Materials Genome Engineering, Beijing Key Laboratory for Science and Application of Functional Molecular and Crystalline Materials, Department of Chemistry and Chemical Engineering, School of Chemistry and Biological Engineering, University of Science and Technology Beijing, Beijing 100083, China. E-mail: d202110468@xs.ustb.edu.cn*

[c] *Key Laboratory of Photochemical Conversion and Optoelectronic Materials, Technical Institute of Physics and Chemistry, Chinese Academy of Sciences, Beijing 100190, China. E-mail: zhengxie@mail.ipc.ac.cn*

3354 | *J. Mater. Chem. C*, 2023, **11**, 3354–3359

This journal is © The Royal Society of Chemistry 2023

Fig. 1   Structures of **COF-MTAPP** and **COF-P-MTAPP**.

Fig. 2   (a) Magnified FT-IR spectra at 1450–1700 cm^{-1}, (b) XRD patterns, experimentally observed (solid line) and simulated (dashed line) (c) solid UV-Vis absorption spectra, and (d) TGA curves of **COF-H$_2$TAPP** and **COF-P-H$_2$TAPP**.
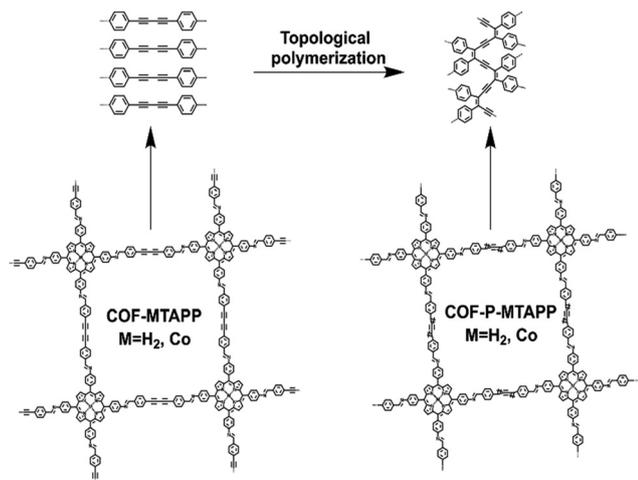
and acetylene bonds, the nonlinear absorption would also be strengthened.[42,43] In the case of porphyrin-based COFs, their NLO properties are believed to be dependent on the dimensionalities, which influences the steric delocalization of the π-conjugated planes. However, the conjugated structure–activity relationship of such materials is still unclear to the best of our knowledge.

In this work, two porphyrin-based 2D COFs **COF-MTAPP** (M = H$_2$, Co) and their corresponding topologically polymerized 3D analogues **COF-P-MTAPP** (M = H$_2$, Co) were synthesized (Fig. 1), and the effects of the degree and orientation of conjugation in porphyrin-based COFs on the NLO properties were discussed for the first time. Theoretical calculation and experimental results showed that **COF-MTAPP** possessed more extended 2D π-conjugation planes, resulting in stronger excited-state absorption (ESA) intensity and higher reverse saturable absorption (RSA) capacity.

Results and discussion

Synthesis and characterization

According to the literature,[44] **COF-H$_2$TAPP** was synthesized by the connection of 5,10,15,20-tetra(4-aminophenyl)-21H,23H porphyrin with 4,4′-(butyl-1,3-diyne-1,4-diyl)diphenylaldehyde (DEBD) using a solvothermal method. The 3D COF **COF-P-H$_2$TAPP** was obtained by covalent coupling of diacetylenyl groups under solid-state topological polymerization(SSTP) conditions at 350 °C. The structures of these COFs were characterized by the local bonding and typical functional groups in the FT-IR spectra (Fig. 2a and Fig. S1, ESI†). After SSTP, the characteristic IR band of the enyne vibration in 3D **COF-P-H$_2$TAPP** appeared at 1510 cm^{-1}, and the characteristic band of C=N vibration was still observed at the same wavenumbers as **COF-H$_2$TAPP**. In addition, due to the conversion of the diacetylenyl group, the C=C stretching of the aromatic ring groups shifted to a higher wavenumber around 1608 cm^{-1}, which was clearly different from that of aryl groups at about 1598 cm^{-1}.
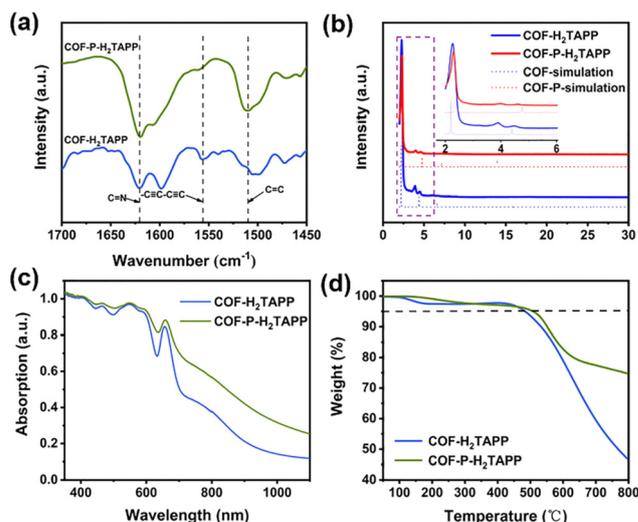
The diacetylene band of **COF-H$_2$TAPP** around 1556 cm^{-1} nearly disappeared in the FT-IR spectra, indicating that almost all units were topological polymerized to the 3D **COF-P-H$_2$TAPP**. The metal-coordinated homologues (**COF-CoTAPP** and **COF-P-CoTAPP**) were prepared by post-synthetic doping of Co ions into the precursor COFs, which was verified by X-ray photoelectron spectroscopy (Fig. S2 and S3, ESI†).

The crystallinity of **COF-H$_2$TAPP** and **COF-P-H$_2$TAPP** was analyzed by powder X-ray diffraction (PXRD) patterns (Fig. 2b). It could be observed that the newly synthesized COFs were polymerized by the Ps manner, of which the PXRD results were consistent with the simulation of the Ps manner (Fig. 2b).[44] The three diffraction peaks at 2.27, 4.52 and 6.19° indicate the high crystallization of **COF-H$_2$TAPP**. In the case of **COF-P-H$_2$TAPP**, these peaks shifted to a wider-angle region, which implied smaller diffraction distances in the interlayer conjugated structures. This is consistent with the reported results.[44] The diffraction fringes in the TEM images with the corresponding SAED patterns also revealed the good crystallinity of the COFs. Moreover, after addition of the Co ions, the crystalline interplanar spacings of the metalloporphyrin-based COFs remained almost the same as their precursors. (Fig. S6 and S7, ESI†). The morphologies of the COFs are illustrated in scanning electron microscopy (SEM) images (Fig. S5, ESI†), from which irregular-shaped nanocrystals with sizes of about 100–300 nm could be observed for all COFs.

In the solid UV-Vis absorption spectra, both 2D COFs exhibited strong absorption in the visible region (Fig. 2c and Fig. S8, ESI†). In comparison, the absorption peak of 3D **COF-P-H$_2$TAPP** showed obvious redshift and leveled-off tails appearing in the long-wavelength region compared to **COF-H$_2$TAPP**, which proved the increase of π–π transitions due to the formation of the enyne chains.[45–47] The thermogravimetric analysis (TGA) curves indicated the excellent thermal stability of the four COFs

This journal is © The Royal Society of Chemistry 2023

J. Mater. Chem. C, 2023, **11**, 3354–3359 | **3355**

with decomposition temperatures (T_ds, corresponding to a 5% weight loss) as high as 500 °C (Fig. 2d and Fig. S9, ESI†), which effectively prevented the thermal decomposition under high energy density for a long time and fulfilled the requirement of the NLO devices. Both **COF-H$_2$TAPP** and **COF-P-H$_2$TAPP** showed permanent porosity at 77 K, which was also effectively conducive to maintaining a stable performance in a wide temperature range. The BET surface areas of four COFs are in the range of 740 to 1171 m^2 g^{-1} (Fig. S10 and S11, ESI†). In the process of aggregation, different positions of the frame would start to polymerize, resulting in the formation of a zigzag structure. This structure would affect the full adsorption of nitrogen molecules on the aromatic edge, thus reducing the measured porosity.[44]

Density function theory (DFT) calculations

The frontier orbitals of the segments of the COFs were calculated using a DFT method, and the results are demonstrated in Fig. S12 and S13 (ESI†).[48] For **COF-H$_2$TAPP**, both the highest occupied molecular orbital (HOMO) and the lowest unoccupied molecular orbital (LUMO) were distributed on the porphyrin and aniline segments, indicating the conjugation nature of the covalent-bonded system. In comparison, the HOMO and the LUMO of **COF-P-H$_2$TAPP** are located on the porphyrin segments, revealing the degree of conjugation between porphyrin layers was increased. The HOMO and LUMO energies of **COF-H$_2$TAPP** are −5.12 and −2.25 eV, respectively. After SSTP, the bandgap was narrowed from 2.87 to 2.65 eV due to the formation of conjugated enyne chains, which was beneficial to the increase of intrinsic carrier concentration.[49] This is also true with **COF-CoTAPP** and **COF-P-CoTAPP**. Introducing metal cobalt into the porphyrin core showed little influence on the conjugated nature of the molecules but resulted in the decrease of the value of HOMO energy and the increase of LUMO energy to −5.21 and −2.15 eV, respectively (Fig. 3).

After SSTP, **COF-P-CoTAPP** showed a narrower bandgap with increasing the HOMO energy level and decreasing the LUMO energy level. This indicates that it promotes the charge transport between layers after SSTP, which facilitates the electronic transition of the ground state.[44]

Third-order nonlinear optical properties

Third-order NLO properties were explored using open aperture Z-scan technology at 532 nm. The samples were dispersed in ethanol by wet grinding and ultrasound to adjust the linear

transmittance to 70%. After ultrasound, TEM images showed that the 2D **COF-MTAPP** were maintained without obvious exfoliation (Fig. S14, ESI†). As shown in Fig. 4, all COFs showed obvious RSA responses. In comparison with 3D **COF-P-MTAPP**, 2D **COF-MTAPP** exhibited smaller normalized transmittance at the focus, indicating that **COF-MTAPP** possessed more powerful RSA intensity. The addition of central coordination metal Co enhanced the RSA intensity, which can be attributed to the extended conjugation within the porphyrin unit and the efficient charge transport process.[50,51] The input–output energy density curves calculated from the corresponding Z-scan curves are shown in Fig. 4f, which reflects a typical OL behavior. The nonlinear absorption coefficient (β) values of **COF-H$_2$TAPP**, **COF-H$_2$TAPP**, **COF-CoTAPP**, **COF-P-H$_2$TAPP** and **COF-P-CoTAPP** were calculated to be 36.25, 38.80, 21.41, 32.68 cm GW^{-1}, respectively. Although the 3D structures showed a higher conjugation degree, the 2D homologs achieved a stronger NLO response, which implied that the steric orientation of the π-conjugated system played a critical role.

The ESA of **COF-MTAPP** and **COF-P-MTAPP** were measured to explain divergences of NLO properties. The excited-state dynamics of both **COF-MTAPP** and **COF-P-MTAPP** were captured in the nanosecond transient absorption spectrum (TAS) in the spectral region of 400–800 nm (Fig. 5). The excitation wavelength was 355 nm, and the decay time constants for the excited state dynamics were obtained. The absorption curves of all COFs exhibited positive absorption ($\Delta OD > 0$), which suggested that ESA curves covered the total spectral region of 400–800 nm and all COFs showed potential applications on the broadband OL response. The peak positions of **COF-MTAPP** and **COF-P-MTAPP** remained consistent with the delay time, which suggested that the ESA originated from the same excited-sate and no other process occurs within the process of ESA.[52] The excited carrier dynamics were obtained simultaneously by TA measurements (Fig. 6). All COFs exhibited long-life processes and the decay curves were single exponential functions, which suggested the radiation processes originated from the single channel process from the single-state to the ground-state.

For **COF-MTAPP**, the addition of central coordination metal Co significantly enhanced peak strength around 532 nm, indicating that it promoted conjugated degrees in the 2D planes of porphyrins to enhance ESA.[52] This may be the reason for the enhanced RSA for **COF-MTAPP**. The absorption peak of **COF-P-MTAPP** around 532 nm was obviously suppressed, which was the result of the conversion from diacetylene to conjugated enyne (Fig. 5). Therefore, for **COF-P-MTAPP**, while π–π conjugated bonds were built between layers to increase the degree of conjugation, the π-conjugated delocalization in the 2D plane was disturbed due to the destruction of the integrity in 2D plane. As a result, the π-conjugated length in the 2D plane would decrease. After interlayered polymerization, the original coplanar diacetylene was converted to twisted enyne chains, which reduced the planar rigidity of the original 2D COF and further reduced its π-conjugation, resulting in the weakening of ESA.[40,41] The 2D **COF-MTAPP** in Fig. 6 showed a longer excited state lifetime, which proved that it had a stronger π-conjugated
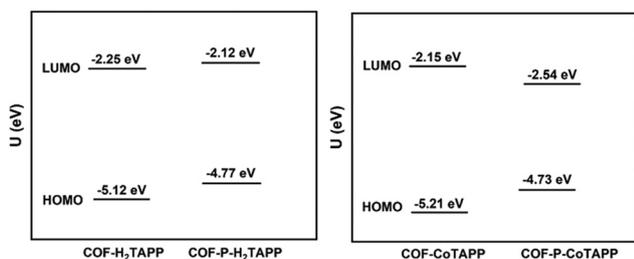
Fig. 3 The energy levels of the HOMO and the LUMO of **COF-MTAPP**, M = H$_2$ and Co, and **COF-P-MTAPP**, M = H$_2$ and Co.
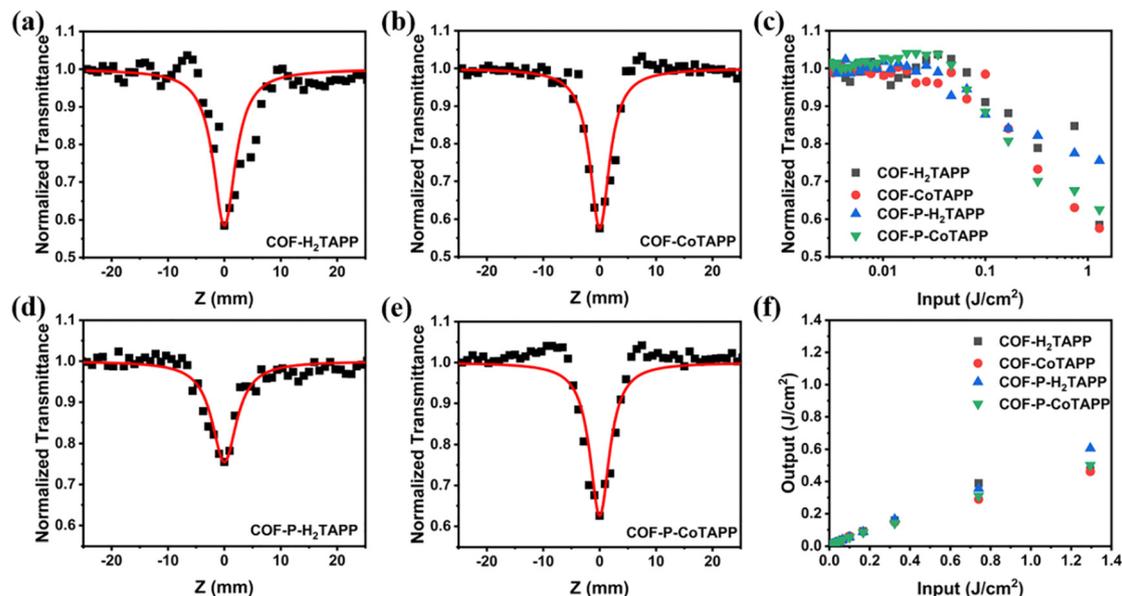
Fig. 4   Normalized transmittance curve of open aperture Z-scan for **COF-MTAPP**, M = H$_2$ (a) and Co (b), and **COF-P-MTAPP**, M = H$_2$ (d) and Co (e) at 10 μJ. The solid lines represent the theoretical fitting, and the squares represent the experimental data. Input–normalized transmittance curves (c) and input−output energy density curves (f) of **COF-MTAPP** and **COF-P-MTAPP** by fitting of the Z-scan curve.
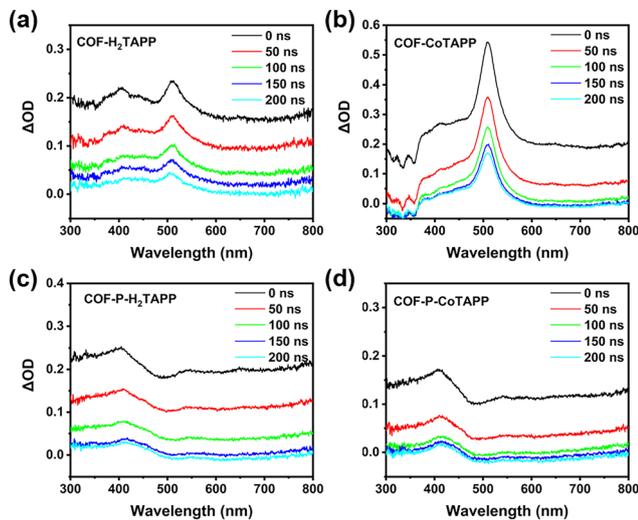

Fig. 5   Nanosecond transient absorption spectra of **COF-MTAPP**, M = H$_2$ (a), Co (b), and **COF-P-MTAPP**, M = H$_2$ (c), Co (d), at different time scales.
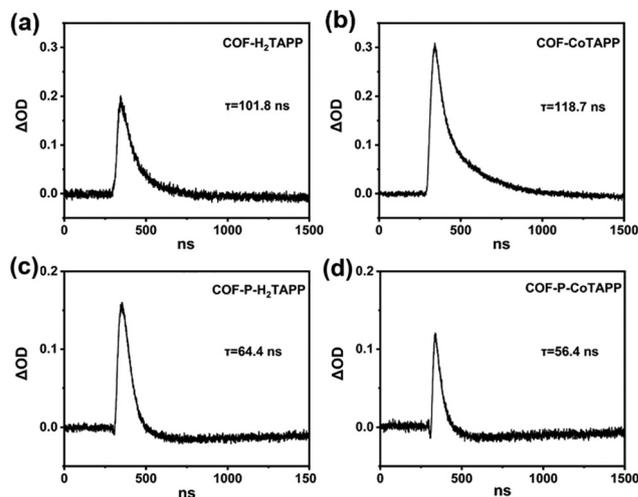

Fig. 6   Dynamics trace of **COF-MTAPP**, M = H$_2$ (a), Co (b), and **COF-P-MTAPP**, M = H$_2$ (c), Co (d), with selected wavelengths of 532 nm.

system to obtain more excited electrons in the excited state, showing a stronger ESA.[53] Thus, the degree of π-conjugation of materials may affect their nonlinear absorption, but it would get worse results at the cost of destroying the original conjugated structures.

Conclusions

In summary, two 2D and two topologically polymerized 3D COFs based on porphyrin building blocks, and diacetylenyl and enynyl linkages were synthesized, respectively, and their NLO

properties were systematically investigated based on the results of Z-scan and nanosecond TAS. The 2D COFs exhibited a stronger RSA signal by the longer π-conjugation length and larger conjugation planes compared to 3D COFs. Moreover, the 2D COFs showed stronger ESA with a longer carrier relaxation life, implying that steric orientations of the π-conjugation of 2D COFs were more favorable for NLO properties. This work focuses on the influence of the steric orientation of the π-conjugation on the NLO properties of porphyrin-based COFs, and provides valuable insights into the modification of optoelectronic performance through the regulation of the dimensionalities of materials.

Conflicts of interest

There are no conflicts to declare.

Acknowledgements

Notes and references

1 L. Xu, J. Sun, T. Tang, H. Zhang, M. Sun, J. Zhang, J. Li, B. Huang, Z. Wang, Z. Xie and W. Y. Wong, *Angew. Chem., Int. Ed.*, 2021, **60**, 11326–11334.
2 L. Lu, W. Wang, L. Wu, X. Jiang, Y. Xiang, J. Li, D. Fan and H. Zhang, *ACS Photonics*, 2017, **4**, 2852–2861.
3 Z. Xie, H. He, Y. Deng, X. Wang and C. Liu, *J. Mater. Chem. C*, 2013, **1**, 1791.
4 Z. Xie, F. Wang and C. Y. Liu, *Adv. Mater.*, 2012, **24**, 1716–1721.
5 L. Wang, H. Xie, Y. Lin, M. Wang, L. Sha, X. Yu, J. Yang, J. Zhao and G. Li, *Biosens. Bioelectron.*, 2022, **217**, 114668.
6 G. Zhang, X. Li, Q. Liao, Y. Liu, K. Xi, W. Huang and X. Jia, *Nat. Commun.*, 2018, **9**, 2785.
7 Z. Wang, Z. Wang, B. Lin, X. Hu, Y. Wei, C. Zhang, B. An, C. Wang and W. Lin, *ACS Appl. Mater. Interfaces*, 2017, **9**, 35253–35259.
8 K. Garg, A. Singh, A. K. Debnath, S. K. Nayak, S. Chattopadhyay, D. K. Aswal, Y. Hayakawa, S. K. Gupta and J. V. Yakhmi, *Chem. Phys. Lett.*, 2010, **488**, 27–31.
9 J. You, Y. Luo, J. Yang, J. Zhang, K. Yin, K. Wei, X. Zheng and T. Jiang, *Laser Photonics Rev.*, 2020, **14**, 2000239.
10 R. Paolesse, S. Nardis, D. Monti, M. Stefanelli and C. Di Natale, *Chem. Rev.*, 2017, **117**, 2517–2583.
11 T. Skorjanc, D. Shetty and M. Valant, *ACS Sens.*, 2021, **6**, 1461–1481.
12 Z. Cai, L. A. Luck, D. Punihaole, J. D. Madura and S. A. Asher, *Chem. Sci.*, 2016, **7**, 4557–4562.
13 Z. Liu, J. Sun, C. Yan, Z. Xie, G. Zhang, X. Shao, D. Zhang and S. Zhou, *J. Mater. Chem. C*, 2020, **8**, 12993–13000.
14 D. Yu, X. Sun, X. Chen, W. Ma, J. Sun, C. Zhou, Z. Xie and S. Zhou, *J. Mater. Chem. C*, 2018, **6**, 5624–5629.
15 Q. Xiao, B. Ma, X. Fei, D. W. Liu, X. P. Zhai, X. Y. Li, M. J. Xiao, Y. Peng, Q. Wang and H. L. Zhang, *Nanoscale Horiz.*, 2021, **6**, 918–927.
16 F. Xing, J. Wang, Z. Wang, Y. Li, X. Gou, H. Zhang, S. Zhou, J. Zhao and Z. Xie, *ACS Appl. Mater. Interfaces*, 2021, **13**, 897–903.
17 J. Sun, B. Yuan, X. Hou, C. Yan, C. Sun, Z. Xie, X. Shao and S. Zhou, *J. Mater. Chem. C*, 2018, **6**, 8495–8501.
18 A. P. Côté, A. I. Benin, N. W.Ockwig, M. O'Keeffe, A. J. Matzger and O. M. Yaghi, *Science*, 2005, **310**, 1166–1170.
19 B. Han, X. Ding, B. Yu, H. Wu, W. Zhou, W. Liu, C. Wei, B. Chen, D. Qi, H. Wang, K. Wang, Y. Chen, B. Chen and J. Jiang, *J. Am. Chem. Soc.*, 2021, **143**, 7104–7113.
20 K. Gottschling, G. Savasci, H. Vignolo-Gonzalez, S. Schmidt, P. Mauker, T. Banerjee, P. Rovo, C. Ochsenfeld and B. V. Lotsch, *J. Am. Chem. Soc.*, 2020, **142**, 12146–12156.
21 J. Feng, Y. Li, Y. Zhang, Y. Xu and X. Cheng, *Chem. Eng. J.*, 2022, **429**, 132499.
22 L. Ding, B. Yao, F. Li, S. Shi, N. Huang, H. Yin, Q. Guan and Y. Dong, *J. Mater. Chem. A*, 2019, **7**, 4689–4698.
23 H. C. Gulbalkan, Z. P. Haslak, C. Altintas, A. Uzun and S. Keskin, *Chem. Eng. J.*, 2022, **428**, 131239.
24 N. Huang, R. Krishna and D. Jiang, *J. Am. Chem. Soc.*, 2015, **137**, 7079–7082.
25 C. Zhang, S. Zhang, Y. Yan, F. Xia, A. Huang and Y. Xian, *ACS Appl. Mater. Interfaces*, 2017, **9**, 13415–13421.
26 P. Peng, L. Shi, F. Huo, S. Zhang, C. Mi, Y. Cheng and Z. Xiang, *ACS Nano*, 2019, **13**, 878–884.
27 X. Feng, X. Ding and D. Jiang, *Chem. Soc. Rev.*, 2012, **41**, 6010–6022.
28 Z. Mu, Y. Zhu, B. Li, A. Dong, B. Wang and X. Feng, *J. Am. Chem. Soc.*, 2022, **144**, 5145–5154.
29 N. Keller and T. Bein, *Chem. Soc. Rev.*, 2021, **50**, 1813–1845.
30 B. Gui, G. Lin, H. Ding, C. Gao, A. Mal and C. Wang, *Acc. Chem. Res.*, 2020, **53**, 2225–2234.
31 Y. Qian, D. Li, Y. Han and H. L. Jiang, *J. Am. Chem. Soc.*, 2020, **142**, 20763–20771.
32 B. P. Biswal, S. Valligatla, M. Wang, T. Banerjee, N. A. Saad, B. M. K. Mariserla, N. Chandrasekhar, D. Becker, M. Addicoat, I. Senkovska, R. Berger, D. N. Rao, S. Kaskel and X. Feng, *Angew. Chem., Int. Ed.*, 2019, **58**, 6896–6900.
33 M. Samal, S. Valligatla, N. A. Saad, M. V. Rao, D. N. Rao, R. Sahu and B. P. Biswal, *Chem. Commun.*, 2019, **55**, 11025–11028.
34 Z. Liu, B. Zhang, Y. Huang, Y. Song, N. Dong, J. Wang and Y. Chen, *iScience*, 2021, **24**, 102526.
35 M. Pawlicki, H. A. Collins, R. G. Denning and H. L. Anderson, *Angew. Chem., Int. Ed.*, 2009, **48**, 3244–3266.
36 K. S. Kim, J. M. Lim, A. Osuka and D. Kim, *J. Photochem. Photobiol., C*, 2008, **9**, 13–28.
37 L. Beverina, M. Crippa, P. Salice, R. Ruffo, C. Ferrante, I. Fortunati, R. Signorini, C. M. Mari, R. Bozio, A. Facchetti and G. A. Pagani, *Chem. Mater.*, 2008, **20**, 3242–3244.
38 L. Ventelon, S. Charier, L. Moreaux, J. Mertz and M. Blanchard-Desce, *Angew. Chem.*, 2001, **113**, 2156–2159.
39 M. Drobizhev, Y. Stepanenko, Y. Dzenis, A. Karotki, A. Rebane, P. N. Taylor and H. L. Anderson, *J. Phys. Chem. B*, 2005, **109**, 7223–7236.
40 O. Mongin, L. Porres, M. Charlot, C. Katan and M. Blanchard-Desce, *Chemistry*, 2007, **13**, 1481–1498.
41 S. Easwaramoorthi, S. Jang, Z. Yoon, J. Lim, C. Lee, C. Mai, Y. Liu, C. Yeh, J. Vura-Weis, M. R. Wasielewski and D. Kim, *J. Phys. Chem. A*, 2008, **112**, 6563–6570.
42 M. Drobizhev, Y. Stepanenko, Y. Dzenis, A. Karotki, A. Rebane, P. N. Taylor and H. L. Anderson, *J. Am. Chem. Soc.*, 2004, **126**, 15352–15353.
43 M. Drobizhev, Y. Stepanenko, Y. Dzenis, A. Karotki, A. Rebane, P. N. Taylor and H. L. Anderson, *J. Phys. Chem. B*, 2005, **109**, 7223–7236.
44 Y. Zhu, P. Shao, L. Hu, C. Sun, J. Li, X. Feng and B. Wang, *J. Am. Chem. Soc.*, 2021, **143**, 7897–7902.

3358 | *J. Mater. Chem. C*, 2023, **11**, 3354–3359

This journal is © The Royal Society of Chemistry 2023

45 Y. Takeoka, K. Asai, M. Rikukawa and K. Sanui, *Chem. Commun.*, 2001, 2592–2593.

46 X. Sun, T. Chen, S. Huang, L. Li and H. Peng, *Chem. Soc. Rev.*, 2010, **39**, 4244–4257.

47 X. You, X. Chen, G. Zou, W. Su, Q. Zhang and P. He, *Chem. Phys. Lett.*, 2009, **482**, 129–133.

48 W. Li, X. Ding, B. Yu, H. Wang, Z. Gao, X. Wang, X. Liu, K. Wang and J. Jiang, *Adv. Funct. Mater.*, 2022, **32**, 2207394.

49 M. A. Green, *J. Appl. Phys.*, 1990, **67**, 2944–2954.

50 D. Dini, M. J. Calvete and M. Hanack, *Chem. Rev.*, 2016, **116**, 13043–13233.

51 P. Tholen, C. A. Peeples, M. M. Ayhan, L. Wagner, H. Thomas, P. Imbrasas, Y. Zorlu, C. Baretzky, S. Reineke, G. Hanna and G. Yucesan, *Small*, 2022, 2204578.

52 J. Kim, J. Oh, A. Osuka and D. Kim, *Chem. Soc. Rev.*, 2022, **51**, 268–292.

53 Y. Han, J. Xiao, X. Wu, W. Zhou, L. Shen, J. Zhang, Y. Wang, X. Zhang and Y. Song, *J. Phys. Chem. B*, 2020, **124**, 10766–10775.